Arab J Sci Eng (2017) 42:3751–3760
DOI 10.1007/s13369-017-2503-5

RESEARCH ARTICLE - CIVIL ENGINEERING

Characteristics of Hydraulic Jump in U-Shaped Channels

Hamed Azimi[1,2] · **Saeid Shabanlou**[3] · **Saeid Kardar**[4]

Received: 7 October 2016 / Accepted: 9 March 2017 / Published online: 17 March 2017

Abstract A hydraulic jump is the rapid transition from a supercritical to subcritical flow. This transition is characterized by large-scale turbulence and energy dissipation. Despite the importance of understanding the hydraulic jump to design hydraulic structures, few studies have aimed on hydraulic jumps in U-shaped channels. In this paper, the 3D pattern of hydraulic jumps in U-shaped channels is studied numerically. The variations of the flow free surface are predicted using the volume of fluid scheme. Also, the flow field turbulence is simulated using the standard $k-\varepsilon$ and RNG $k-\varepsilon$ turbulence models. According to the numerical modeling results, the standard $k-\varepsilon$ turbulence model estimates the flow characteristics with more accuracy. A comparison between the laboratory and numerical results shows that the numerical model simulates the flow field characteristics with good accuracy. For example, in the hydraulic jump model with a relative discharge ($q = Q/\sqrt{(gD^5)}$) equal to 0.321 and a Froude number (F_1) equal to 4.85, the values of MAPE, RMSE and R^2 are calculated 7.617, 0.022 and 0.989, respectively. Next, 45 numerical models are simulated in different hydraulic conditions and some relationships are provided for calculating the sequent depth (h_2/h_1), hydraulic length (L_j/h_1) and roller length (L_r/h_1) ratios by analyzing their results.

Keywords Hydraulic jump · U-shaped channels · Numerical simulation · Flow free surface

✉ Saeid Shabanlou
Saeid.shabanlou@gmail.com

Hamed Azimi
Azimi86Hamed@gmail.com

Saeid Kardar
kardar1976@yahoo.com

[1] Department of Civil Engineering, Razi University, Kermanshah, Iran

[2] Water and Wastewater Research Center, Razi University, Kermanshah, Iran

[3] Department of Water Engineering, Kermanshah Branch, Islamic Azad University, Kermanshah, Iran

[4] Department of Environmental Engineering, College of Environment and Energy, Science and Research Branch, Islamic Azad University, Tehran, Iran

List of symbol

A_x, A_y, A_z	Fractional areas open to flow (−)
CDIS1	Coefficient of production (−)
CDIS2	Coefficient of decay (−)
CDIS3	is coefficient of buoyancy (−)
D	U-shaped channel diameter (L)
Diff_T	Diffusion term (−)
$\mathrm{Diff}_\varepsilon$	Diffusion of dissipation (−)
F	Fluid volume fraction in a cell (−)
F_1	Froude number at upstream of hydraulic jump (−)
f_x, f_y, f_z	Viscous accelerations (−)
G_x, G_y, G_z	Body accelerations (−)
G_T	Turbulence production due to buoyancy effects (−)
g	Acceleration gravity ($\mathrm{L\,T^{-2}}$)
k_T	Turbulence kinetic energy ($\mathrm{L^2\,T^{-2}}$)
L_j	Length of hydraulic jump (L)
L_r	Roller length (L)
p	Pressure ($\mathrm{M\,L^{-1}\,T^{-2}}$)
P_T	Turbulent kinetic energy production (−)
Q	Discharge in U-shaped channel ($\mathrm{L^3\,T^{-1}}$)
q	Relative discharge (−)
R	Mass source (−)

t	Time (T)
u, v, w	Velocity components ($\mathrm{L\,T^{-1}}$)
u_*	Wall shear velocity ($\mathrm{L\,T^{-1}}$)
V_F	Fractional volume open to flow (−)
x, y, z	Cartesian coordinate directions (L)
y_1	Distance of the cell center from the solid wall (L)
y^+	Non-dimensional parameter (−)
h_1	Depth of flow at upstream of hydraulic jump (L)
h_2	Depth of the flow at downstream of hydraulic jump (L)
μ	Water viscosity ($\mathrm{M\,L^{-1}\,T^{-1}}$)
ε_T	Turbulence dissipation rate ($\mathrm{L^2\,T^{-3}}$)
ν	Kinematic viscosity ($\mathrm{L^2\,T^{-1}}$)
ρ	Fluid density ($\mathrm{M\,L^{-3}}$)

1 Introduction

The rapid transition from a supercritical to subcritical flow is characterized by large-scale turbulence and energy dissipation. This transition is called a hydraulic jump. The hydraulic jump is a type of rapidly varied flows and used for water chlorination in treatment plants and energy dissipation of the flow and other hydraulic purposes. Generally, a hydraulic jump is created after control gates, weirs and ogee spillways. Many experimental, analytical and numerical studies have been carried out on field due to the importance and complex structure of this phenomenon.

Most of the studies carried out on the hydraulic jump include the formation of the hydraulic jump in rectangular channels. Rouse et al. [1], Rao and Rajaratnam [2], McCorquodale [3], Long et al. [4], Svendsen et al. [5], Liu and et al. [6] are researchers who investigated the hydraulic jump characteristics in rectangular channels. In contrast, different studies have been conducted on the hydraulic jump in non-rectangular channels. Hager [7] studied the hydraulic jump behavior in a rectangular, horizontal and non-prismatic channel. Hager and Wanoschek [8] analytically studied the hydraulic jump characteristics in triangular channels. They investigated the sequent depth ratio, the roller length and the jump length for different Froude numbers. Debabeche et al. [9] experimentally and theoretically studied hydraulic jumps in triangular channels with central angle of 90°. They introduced an analytical relationship for a triangular channel inflow Froude number. Their relationship predicts the Froude number as a function of the sequent depth ratio and the channel slope. Vatankhah and Omid [10] introduced an analytical method for analyzing the hydraulic jump in horizontal triangular channels. Their solution predicts the sequent depth ratio using the specific force equation. Rashwan [11] theoretically studied the hydraulic jump characteristics in a horizontal triangular channel and provided an analytical method based on the momentum principles. In the next sections, some conducted studies on hydraulic jumps in trapezoidal channels are reviewed. Wanoschek and Hager [12] by a laboratory study investigated the hydraulic jump characteristics in trapezoidal channels. They analyzed the flow free surface changes, the sequent depth ratio and the velocity field. Afzal and Bushra [13] investigated the turbulent structure of hydraulic jumps in trapezoidal channels. They provided a relationship for calculating the hydraulic jump length by assuming the flow as two dimensional and using the Reynolds equations.

Study of the hydraulic jump in circular channels and U-shaped channels has been also carried out by some researchers. Hager [14] performed an analytical and experimental study to analysis the hydraulic jump in U-shaped and circular channels. Using the momentum equations, he obtained the sequent depth ratio for various Froude numbers. He experimentally studied the flow free surface variations, the roller length and the velocity vectors of the hydraulic jump in a U-shaped channel. Stahl and Hager [15] by conducting an experimental study measured the sequent depths of the hydraulic jump in a circular channel for different Froude numbers. The range of the Froude numbers of their study was from 1.5 to 6.5. Bushra and Afzal [16], by assuming the flow as two dimensional investigated the turbulent structure of hydraulic jumps in circular and U-shaped channels using the Reynolds equations and introduced a method for predicting the sequent depth ratio of hydraulic jumps.

Ghomri and Riguet [17] carried out an experimental study on the hydraulic jump in a U-shaped channel with rough bed. They presented an equation as a function of the relative roughness and the discharge to estimate the length of the hydraulic jump on the rough bed. Zhang and Li [18] presented an analytical solution to calculate the critical depth, the Froude number and the hydraulic jump in U-shaped channels. Houichi et al. [19] investigated the hydraulic jump characteristics in U-shaped channels in an experimental and numerical study using the artificial neural network. They proposed an equation to compute the relative length of the hydraulic jump (L_j/h_1) as follows:

$$\frac{L_\mathrm{j}}{h_1} = 113.8 + 967.21q - 485.03h_1 + 12.35F_1 - 266.29h_2 \tag{1}$$

where L_j is the length of the hydraulic jump, h_1 is the flow depth at the upstream of the hydraulic jump, q is the relative discharge ($Q/\sqrt{(gD^5)}$), F_1 is the Froude number at the upstream of the hydraulic jump, h_2 is the flow depth at the downstream of the hydraulic jump.

In recent years, numerical models have been widely used for simulating the flow field. Also, many numerical studies have been carried out on hydraulic jumps. Abdel-Gawad

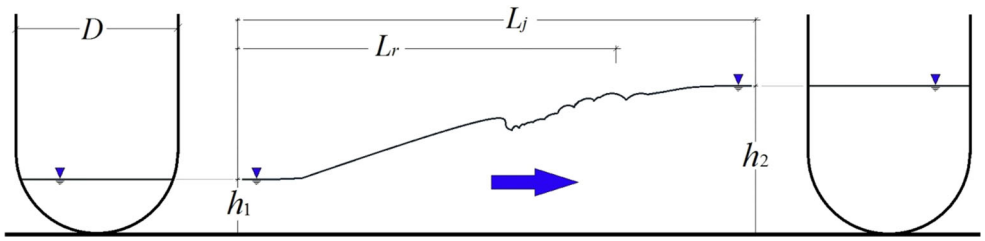

Fig. 1 Schematic of hydraulic jump in U-shaped channel used in Hager experimental model

and McCorquodale [20] numerically studied the characteristics of submerged radial hydraulic jumps in submergence different conditions. They solved the continuous and momentum equations using the strip integral method. Sakarya and Tokyay [21] simulated the flow pattern of the hydraulic jump passing over a positive step in horizontal and rectangular channels. Zhao et al. [22] simulated the flow field turbulence of hydraulic jumps in rectangular channels using the standard $k-\varepsilon$ and $k-l$ turbulence models. They simulated the free surface changes using the volume of fluid scheme. Federico et al. [23] simulated the hydraulic jump as two dimensional and using the SPH model. Rostami et al. [24] modeled the flow field of undular hydraulic jumps using FLOW-3D. They used the VOF method to predict the flow free surface changes.

Numerical simulation techniques have widely been used in simulating engineering phenomena [25–30]. According to the literature, despite the importance of understanding the hydraulic jump to design hydraulic structures, few experimental and analytical studies have aimed on hydraulic jumps in U-shaped channels. According to the authors' knowledge, no study has been carried out on the application of numerical methods for simulating the flow field in U-shaped channels, so far. In this study, a numerical study is presented to model the turbulence of the flow field in U-shaped channels for first time.

In this study, the flow pattern of hydraulic jumps in U-shaped channels is simulated using the FLOW-3D software. The FLOW-3D model is a valid simulation tool which provides valuable insights into real flow processes for design purposes, with particular capabilities for accurate modeling the turbulent flows and the dynamic free surface [31].Turbulence of the flow field is simulated using the standard $k-\varepsilon$ and RNG $k-\varepsilon$ turbulence models and the flow free surface changes are simulated using the volume of fluid (VOF) scheme. The VOF scheme is used in the FLOW-3D model for predicting the flow free surface. The VOF scheme consists of three main components: the determination of the volume of fluid function, a procedure to solve the VOF transport equation and setting the boundary conditions at the free surface [31].

The main purpose of this study is providing a 3D numerical model of the flow free surface variations when a hydraulic jump occurs in U-shaped channels. To this end, 45 numerical models are run after model verification and some relationships are provided for determining the sequent depth, jump length and roller length ratios by analyzing the numerical model results.

Table 1 Range of hydraulic parameters used in Hager experimental model

Parameter	Q (m^3/s)	h_1 (m)	h_2(m)	F_1 (−)
Range	0.0079–0.0794	0.0265–0.137	0.101–0.339	1.93–8.85

2 Experimental Model

In this study, for verifying the numerical model results the measurements obtained by Hager [14] are used. Hager's laboratory model is composed of an open U-shaped channel with a length of 8 m made of aluminum sheet. The U-shaped channel width is 0.3 m, and the bed slope of all Hager's laboratory models is set equal to 0.003. In Fig. 1, the schematic of the hydraulic jump in the U-shaped channel of Hager's model is illustrated. In this figure, D is the U-shaped channel width, h_1 is the flow depth at the hydraulic jump upstream, h_2 is the flow depth at the hydraulic jump downstream, Q is the discharge in the U-shaped channel, L_j is the hydraulic jump length, and L_r is the length of the roller. Generally, the horizontal distance between the h_1 and h_2 is called the "hydraulic jump length (L_j)." The horizontal distance between the toe of the hydraulic jump and the end of the roller where the flow depth is equal to h_1 is defined as the roller length (L_r). In Table 1, the range of the hydraulic parameters of Hager's experimental model is provided.

3 Methodology

3.1 Governing Equations

In the FLOW-3D model, the Navier–Stokes and continuity equations are discretized using the finite difference method. The computational domain is divided into a mesh of rectangular cells. All variables (except for velocity values) are

placed at the center of the computational cells (staggered grid arrangement). To solve the governing equations, control volumes are defined around each dependent variable. The surface fluxes, body forces and surface stresses were computed in terms of surrounding variables. Most terms in the governing equations are explicitly evaluated. To solve the flow field of a non-compressible fluid, the continuity and the Navier Stocks equations are solved as follows [31]:

$$V_F\frac{\partial \rho}{\partial t}+\frac{\partial\left(\rho u A_x\right)}{\partial x}+\frac{\partial\left(\rho v A_y\right)}{\partial y}+\frac{\partial\left(\rho w A_z\right)}{\partial z}=R_{SOR} \tag{2}$$

$$\frac{\partial u}{\partial t}+\frac{1}{V_F}\left(uA_x\frac{\partial u}{\partial x}+vA_y\frac{\partial u}{\partial y}+wA_z\frac{\partial u}{\partial z}\right)=-\frac{1}{\rho}\frac{\partial p}{\partial x}+G_x+f_x \tag{3}$$

$$\frac{\partial v}{\partial t}+\frac{1}{V_F}\left(uA_x\frac{\partial v}{\partial x}+vA_y\frac{\partial v}{\partial y}+wA_z\frac{\partial v}{\partial z}\right)=-\frac{1}{\rho}\frac{\partial p}{\partial y}+G_y+f_y \tag{4}$$

$$\frac{\partial w}{\partial t}+\frac{1}{V_F}\left(uA_x\frac{\partial w}{\partial x}+vA_y\frac{\partial w}{\partial y}+wA_z\frac{\partial w}{\partial z}\right)=-\frac{1}{\rho}\frac{\partial p}{\partial z}+G_z+f_z \tag{5}$$

where (u, v, w), (A_x, A_y, A_z), (G_x, G_y, G_z) and (f_x, f_y, f_z) are the velocity components, the fractional area open to the flow, the gravitational force and accelerations due to the viscosity in the x, y and z directions, respectively. Also, t, ρ, R, p and V_F are the time, the density, the mass source, the pressure and the fractional volume open to the flow, respectively [31].

and water phases. In this study, the VOF method is used to predict the variations of the flow free surface. In this method for calculating the fluid volume component, the following equation is calculated:

$$\frac{\partial F}{\partial t}+\frac{1}{V_F}\left(\frac{\partial}{\partial x}(FuA_x)+\frac{\partial}{\partial y}(FvA_y)+\frac{\partial}{\partial z}(FwA_z)\right)=0.0. \tag{6}$$

4 Boundary Conditions

The applied boundary conditions are based on the physical model of Hager's experimental study. Therefore, the depth and discharge certain values are used due to the availability of this data. At the outlet section of the U-shaped channel, the depth and flow certain values are used. All the solid walls of the U-shaped channel are defined as the "Wall boundary conditions." Also, a symmetry plane is determined at the top layer of the computation field.

4.1 Computational Domain and Grid Layout

To estimate the accuracy of the numerical model, statistical indices such as the mean absolute percentage error (MAPE), the root-mean-square error (RMSE) and the correlation coefficient (R^2) are used:

$$\mathrm{MAPE}=\frac{1}{n}\sum_{i=1}^{n}\left(\frac{\left|(R)_{(\mathrm{Predicted})_i}-(R)_{(\mathrm{Observed})_i}\right|}{(R)_{(\mathrm{Observed})_i}}\right)\times 100 \tag{7}$$

$$\mathrm{RMSE}=\sqrt{\frac{1}{n}\sum_{i=1}^{n}\left((R)_{(\mathrm{Predicted})_i}-(R)_{(\mathrm{Observed})_i}\right)^2} \tag{8}$$

$$R^2=\frac{\left(n\sum_{i=1}^{n}(R)_{(\mathrm{Predicted})_i}(R)_{(\mathrm{Observed})_i}-\sum_{i=1}^{n}(R)_{(\mathrm{Predicted})_i}\sum_{i=1}^{n}(R)_{(\mathrm{Observed})_i}\right)^2}{\left(n\sum_{i=1}^{n}\left((R)_{(\mathrm{Predicted})_i}\right)^2-\sum_{i=1}^{n}\left((R)_{(\mathrm{Predicted})_i}\right)^2\right)\left(n\sum_{i=1}^{n}\left((R)_{(\mathrm{Observed})_i}\right)^2-\sum_{i=1}^{n}\left((R)_{(\mathrm{Observed})_i}\right)^2\right)} \tag{9}$$

In numerical simulations of the flow field, the ability to predict the flow free surface is very important. One of the most important methods is volume of fluid (VOF) which simulates the flow field free surface using the interface capturing method. This method was suggested by Hirt and Nichols [32] for the first time. Hirt and Nichols [32] showed the fluid volume component in each cell by the parameter F. They stated that if $F = 0$, the cell is empty, if $F = 1$, the cell is filled with the fluid, and if $0 < F < 1$, the cell contains both air

where $R_{(\mathrm{Predicted})}$ and $R_{(\mathrm{Observed})}$ are the experimental and numerical results, respectively, and n is the number of the experimental measurements. In this study, a U-shaped channel is defined with a length of 8 m, a height of 0.4 m and a width of 0.3 m. The distance from the first cell is chosen somehow to avoid from calculations below the viscose zone. For this purpose, the first node is located where the dimensionless parameter y^+ which is defined based on Eq. (10) be >30:

Table 2 Gridding characteristics, MAPE, RMSE and R^2 of flow free surface changes for model with q of 0.321 and Froude number of 4.85

Meshing	Number of cells	MAPE	RMSE	R^2
1	550000	9.235	0.031	0.957
2	825000	8.438	0.0271	0.969
3	**1190700**	**7.617**	**0.022**	**0.989**
4	1423500	7.025	0.0199	0.990
5	1660750	7.023	0.0198	0.990

Gridding chosen for the separation of the flow field is indicated in bold

$$y^+ = \frac{y_1 u_*}{v} \tag{10}$$

where y_1 is the first node distance from the wall perpendicular to it, u_* is the wall shear stress, and v is the kinematic viscosity of the fluid. The entire computational domain is gridded by a non-uniform mesh block. In Table 2, the characteristics of an example gridding used in the simulation of the flow free surface changes for a model with a relative discharge of 0.454 and the Froude number of 4.85 are provided.

For the coarse mesh (mesh number 1), the MAPE, RMSE and R^2 are estimated 9.235, 0.031 and 0.957, respectively. Also, for the fine mesh (mesh number 5) the statistics indices are calculated 7.023, 0.0198 and 0.990, respectively. Therefore, the error values are decreased with increasing the number of the computational cells. According to numerical simulation results, the difference between the results of griddings 3 and 4 is negligible and gridding 3 is chosen for the separation of the flow field. Therefore, the U-shaped channel is separated in the x, y and z directions by 350, 54 and 63 cells, respectively. The used gridding in the numerical simulation is shown in Fig. 2.

5 Turbulence Model

In this study, the standard $k-\varepsilon$ and RNG $k-\varepsilon$ turbulence models are used to simulate the flow field turbulence. For both $k-\varepsilon$ and RNG $k-\varepsilon$ turbulence models, the turbulent kinetic energy (k_T) and the turbulence dissipation (ε_T) have been solved using the following equations [31]:

$$\frac{\partial k_T}{\partial t} + \frac{1}{V_F}\left\{uA_x\frac{\partial k_T}{\partial x} + vA_y\frac{\partial k_T}{\partial y} + A_z\frac{\partial k_T}{\partial z}\right\} = P_T + G_T + \mathrm{Diff}_T - \varepsilon_T \tag{11}$$

$$\frac{\partial \varepsilon_T}{\partial t} + \frac{1}{V_F}\left\{uA_x\frac{\partial \varepsilon_T}{\partial x} + vA_yR\frac{\partial \varepsilon_T}{\partial y} + wA_z\frac{\partial \varepsilon_T}{\partial z}\right\} = \frac{\mathrm{CDIS1}\cdot\varepsilon_T}{k_T}(P_T + \mathrm{CDIS3}\cdot G_T) + \mathrm{Diff}_\varepsilon - \mathrm{CDIS2}\frac{\varepsilon_T^2}{k_T} \tag{12}$$

where P_T is the turbulent kinetic energy formation, G_T is the turbulence formation due to the buoyancy effects, Diff_T is the diffusion term, $\mathrm{Diff}_\varepsilon$ is the diffusion of dissipation, CDIS1 is the coefficient of formation, CDIS2 is the coefficient of decay, and CDIS3 is the coefficient of buoyancy.

The simulation results of the free surface changes for the standard $k-\varepsilon$ and RNG $k-\varepsilon$ turbulence models are illustrated in Fig. 3. In Table 3, the values of MAPE, RMSE and

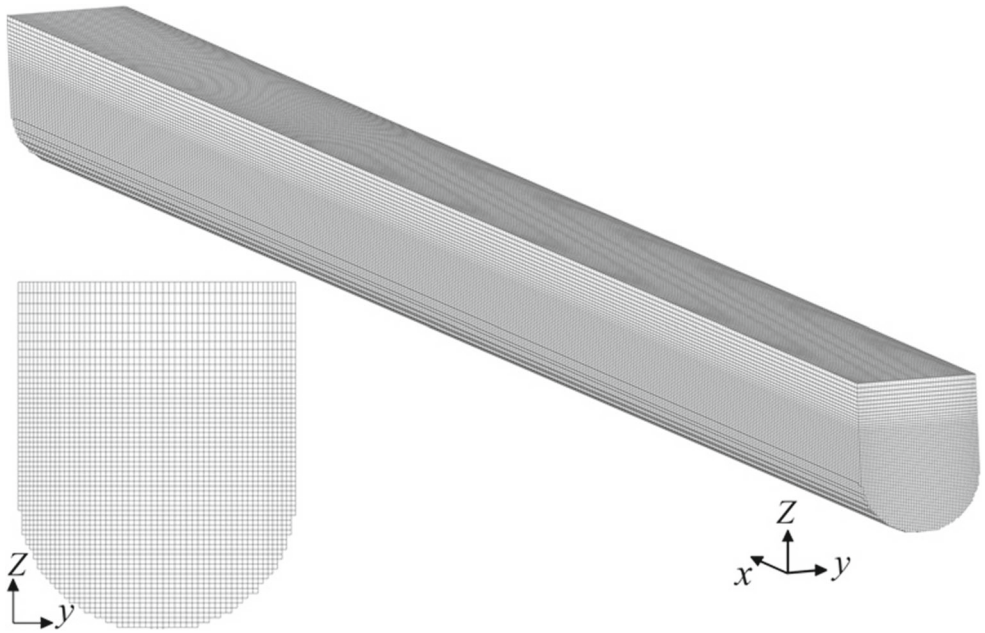

Fig. 2 Used gridding in flow field separation

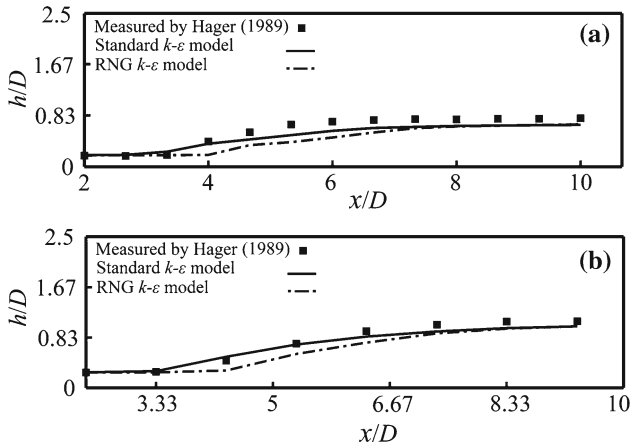

Fig. 3 Prediction of flow free surface changes for standard $k-\varepsilon$ and RNG $k-\varepsilon$ turbulence models **a** $q = 0.166$, $F_1 = 5.3$ **b** $q = 0.321$, $F_1 = 4.85$

Table 3 Values of MAPE, RMSE and R^2 for standard $k-\varepsilon$ and RNG $k-\varepsilon$ turbulence models

	Turbulence model	MAPE	RMSE	R^2
$q = 0.334$, $F_1 = 5.3$	Standard $k-\varepsilon$	16.066	0.032	0.975
	RNG $k-\varepsilon$	21.393	0.049	0.856
$q = 0.454$, $F_1 = 4.85$	Standard $k-\varepsilon$	7.617	0.022	0.989
	RNG $k-\varepsilon$	14.402	0.039	0.966

R^2 turbulence models are shown. For the hydraulic jump with $q = 0.166$, $F_1 = 5.3$, the standard $k-\varepsilon$ turbulence model predicts the values of MAPE, RMSE and R^2 equal to 16.066, 0.032 and 0.975, respectively. In contrast, the RNG $k-\varepsilon$ turbulence model calculates these values (MAPE, RMSE and R^2) equal to 21.393, 0.049 and 0.856, respectively. As a result, the RNG $k-\varepsilon$ turbulence model predicts the correlation coefficient about 12% less than the standard $k-\varepsilon$ turbulence model. Also, for the hydraulic jump with $q = 0.321$, $F_1 = 4.85$ the standard $k-\varepsilon$ turbulence model estimates the MAPE value equal to 7.617 and the values of RMSE and the correlation coefficient are calculated 0.022 and 0.989, respectively. For this hydraulic jump, these values (MAPE, RMSE and R^2) are estimated by the RNG $k-\varepsilon$ turbulence model 14.402, 0.039 and 0.966, respectively. The MAPE value for the RNG $k-\varepsilon$ turbulence model is almost 1.9 times the standard $k-\varepsilon$turbulence model. As shown, the standard $k-\varepsilon$ turbulence model has more accuracy. Therefore, it is used for predicting the flow field turbulence.

6 Validation

A comparison between the flow free surface variations for the results of the numerical model validation with the exper-

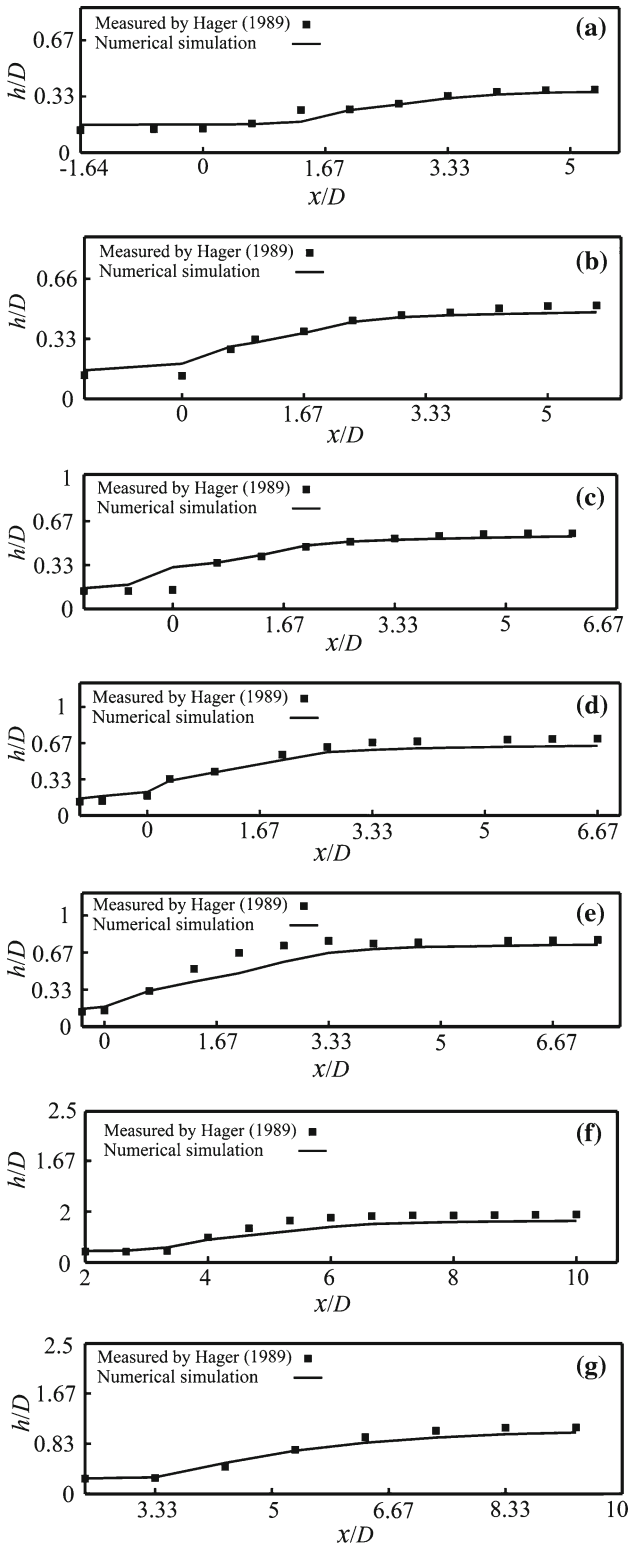

Fig. 4 Comparison between simulated flow free surface with experimental results **a** $q = 0.063$, $F_1 = 3.3$. **b** $q = 0.083$, $F_1 = 4.65$. **c** $q = 0.096$, $F_1 = 5.35$. **d** $q = 0.115$, $F_1 = 6.6$. **e** $Q = 0.128$, $F_1 = 7.15$. **f** $q = 0.166$, $F_1 = 5.3$. **g** $q = 0.321$, $F_1 = 4.85$

Table 4 Values of MAPE, RMSE and R^2 for different hydraulic jump models in U-shaped channel

Model	MAPE	RMSE	R^2
$q = 0.164$, $F_1 = 3.3$	9.904	0.008	0.925
$q = 0.223$, $F_1 = 4.65$	10.497	0.009	0.988
$q = 0.258$, $F_1 = 5.35$	16.506	0.016	0.936
$q = 0.315$, $F_1 = 6.6$	12.070	0.015	0.998
$q = 0.344$, $F_1 = 7.15$	13.093	0.026	0.941
$q = 0.334$, $F_1 = 5.3$	16.066	0.032	0.975
$q = 0.454$, $F_1 = 4.85$	7.617	0.022	0.989

imental measurements are shown in Fig. 4. Also, the values of MAPE, RMSE and R^2 for different hydraulic jump models are provided in Table 4. For the hydraulic jump model with $q = 0.063$, $F_1 = 3.3$, the values of MAPE and RMSE are calculated 9.904 and 0.008, while the correlation coefficient is obtained 0.925. The values of MAPE, RMSE and R^2 for the hydraulic jump model with $q = 0.083$, $F_1 = 4.65$ are calculated 10.497, 0.009 and 0.988, respectively. Also, for the hydraulic jump models with $q = 0.096$, $F_1 = 5.35$ and $q = 0.115$, $F_1 = 6.6$, the values of MAPE are predicted 16.506 and 12.070, respectively. RMSE and the correlation coefficient for the hydraulic jump model with $q = 0.128$, $F_1 = 7.15$ are estimated 0.026 and 0.941, respectively. Furthermore, for the hydraulic jump model with $q = 0.166$, $F_1 = 5.3$, the value of R^2 is calculated 0.975 and for the model with $q = 0.321$, $F_1 = 4.85$, this statistical index is estimated 0.989. Considering the statistical indices calculated for different hydraulic jump models in U-shaped channel, the numerical model predicts the flow free surface changes with good accuracy.

7 Sequent Depth, Length Ratio and Roller Length

In an open channel with a width of D, the effective parameters on the hydraulic jump are: the gravity acceleration (g), the water density (ρ), the flow depth at the hydraulic jump upstream (h_1), the flow depth at the hydraulic jump downstream (h_2), the flow discharge (Q) and the water viscosity (μ). Also, f is the function symbol:

$$f(g, \rho, h_1, h_2, Q, D, \mu) = 0 \tag{13}$$

By assuming that the flow viscosity and the density are constant and the Froude number is equal to F_1 when the hydraulic jump occurs, Eq. (13) is written as follows:

$$f(F_1, h_2/h_1) = 0 \tag{14}$$

Therefore, the effective parameters on the sequent depth (h_2/h_1), hydraulic length (L_j/h_1) and the roller length (L_r/h_1) ratios are:

$$\frac{h_2}{h_1} = f(F_1) \tag{15}$$

$$\frac{L_j}{h_1}, \frac{L_r}{h_1} = f(F_1, h_2/h_1) \tag{16}$$

Then, 45 hydraulic jump models in U-shaped channels are simulated in various hydraulic conditions. In each numerical model, the hydraulic jump characteristics such as the Froude number, the jump length (L_j/h_1), the roller length (L_r/h_1) and the sequent depth (h_2/h_1) ratios are calculated and the results are provided in Table 5. In Fig. 5, the comparison between the sequent depths and the hydraulic jump length ratios with Hager's experimental values are shown.

Table 5 Results of hydraulic jump characteristics for different numerical models

F_1	L_j/h_1	L_r/h_1	h_2/h_1	F_1	L_j/h_1	L_r/h_1	h_2/h_1	F_1	L_j/h_1	L_r/h_1	h_2/h_1
4.85	26.315	7.895	4.368	6.45	35.307	18.936	5.929	4.65	27.042	12.953	4.598
5.30	28.846	13.462	4.346	7.40	38.831	21.313	6.631	5.05	28.678	14.096	4.894
3.30	25.714	14.286	3.286	8.45	42.383	23.620	7.406	5.30	29.633	14.748	5.079
4.65	21.428	14.286	3.881	8.85	45.667	26.298	7.702	5.70	32.484	17.022	5.374
5.35	35.294	20.588	5.176	6.90	37.654	20.693	6.261	6.10	34.312	18.343	5.670
6.60	36.363	20.779	5.377	3.30	18.014	5.833	3.601	6.50	36.686	20.173	5.966
7.15	45.454	27.273	6.970	4.65	26.128	12.103	4.598	2.40	14.690	3.595	2.936
5.37	37.083	20.833	4.792	5.35	29.896	14.945	5.116	3.05	18.507	6.529	3.416
3.53	26.667	13.333	4.167	6.60	36.570	19.969	6.039	3.30	19.901	7.590	3.601
6.27	36	24	6.200	7.15	39.351	22.035	6.446	3.80	22.729	9.747	3.970
4.62	26.667	16.667	5.333	2.35	14.132	3.122	2.899	4.15	24.774	11.318	4.229
4.24	22.8577	12.286	4.571	2.75	16.614	5.052	3.194	4.85	28.575	14.191	4.746
3.43	22.500	7.500	3.750	3.15	18.761	6.671	3.490	1.93	12.357	1.869	2.588
5.12	31.429	17.143	4.857	3.65	22.261	9.454	3.859	2.28	14.481	3.514	2.847
5.10	37.143	20	5.714	4.05	23.817	10.521	4.154	2.50	15.925	4.649	3.010

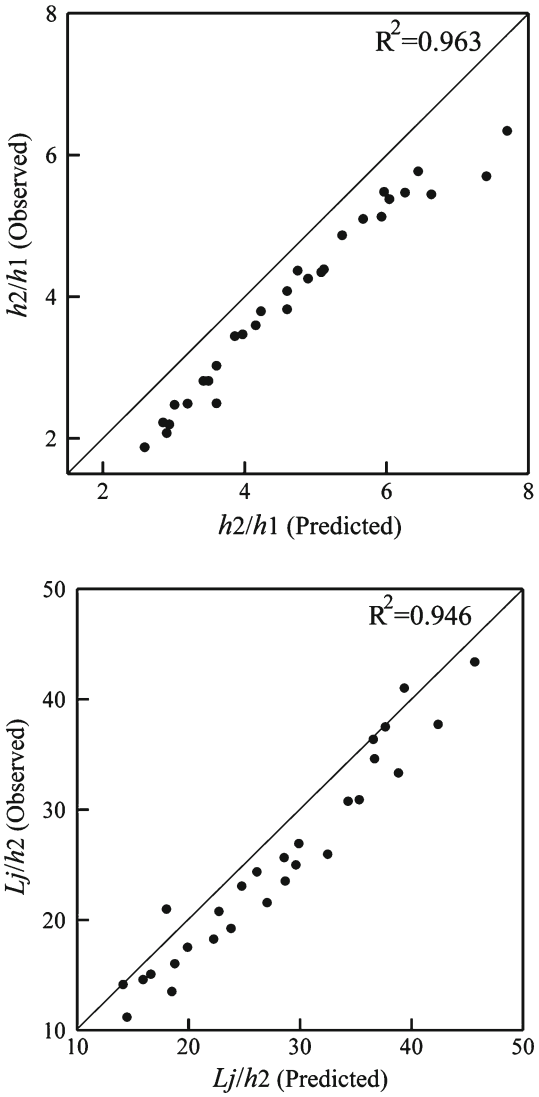

Fig. 5 Comparison between predicted and observed values of h_2/h_1 and L_j/h_1

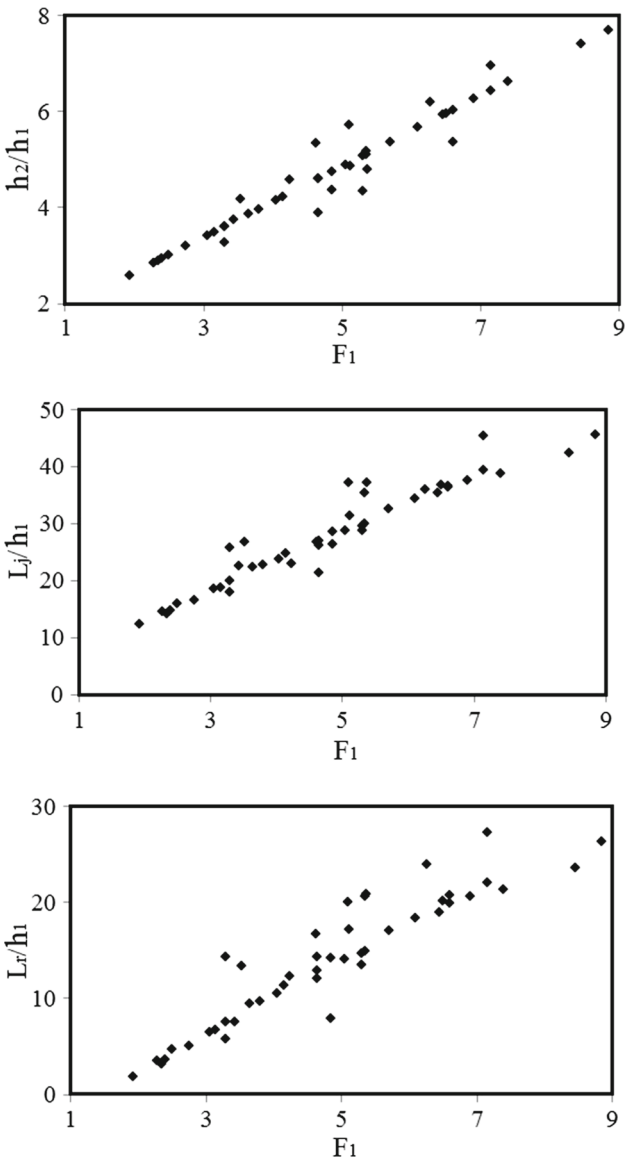

Fig. 6 Variations of sequent depth, jump length and roller length ratios versus Froude number

The MAPE value for the sequent depth ratio is calculated 20.006. Also, the numerical model predicts the values of RMSE and the correlation coefficient for h_2/h_1 0.772 and 0.963, respectively. In contrast, for the hydraulic jump length ratio (L_j/h_1), the values of MAPE, RMSE and R^2 are calculated 16.659, 3.606 and 0.946, respectively. In this study, the sensitivity of different numerical models is investigated in terms of the discrepancy ratio (DR). The discrepancy ratio is introduced as the ratio of the predicted values to the experimental measurements:

$$\mathrm{DR} = (R)_{(\mathrm{Predicted})}/(R)_{(\mathrm{Observed})} \tag{17}$$

The values of the maximum, minimum and average discrepancy ratios ($\mathrm{DR}_{(\mathrm{max})}$, $\mathrm{DR}_{(\mathrm{min})}$, $\mathrm{DR}_{(\mathrm{ave})}$) are calculated for the h_2/h_1 and L_j/h_1 values. According to the results, $\mathrm{DR}_{(\mathrm{max})}$ for the h_2/h_1 parameter is calculated 1.444 and $\mathrm{DR}_{(\mathrm{min})}$ and $\mathrm{DR}_{(\mathrm{ave})}$ are predicted 1.086 and 1.200, respectively. $\mathrm{DR}_{(\mathrm{max})}$, $\mathrm{DR}_{(\mathrm{min})}$ and $\mathrm{DR}_{(\mathrm{ave})}$ for the L_j/h_1 parameter are obtained 1.668, 0.858 and 1.154, respectively. Therefore, the numerical model predicts the sequent depth ratio and jump length values with good accuracy.

The changes in the sequent depth (h_2/h_1), the jump length (L_j/h_1) and the roller length (L_r/h_1) ratios versus the Froude number of different numerical models are illustrated in Fig. 6. According to this Figure, all three hydraulic parameters, h_2/h_1, L_j/h_1 and L_r/h_1 increase with increasing the flow Froude number. As shown, in this study the changes in the parameters cover the range of Froude numbers from 1.93 to 8.85. In the following, some relationships are provided

Table 6 Values of MAPE, RMSE and R^2 for numerical model and Houichi et al.'s equation

Equation	MAPE	RMSE	R^2
1	1242.576	244.050	0.05
19	16.659	3.606	0.946

for the sequent depth, jump length and roller length ratios by analyzing the numerical models results using the nonlinear regression. The relationship of the sequent depth ratio in terms of the Froude number of the hydraulic jump upstream, the relationship of the hydraulic jump length ratio and the relationship of the roller length ratio are introduced as a function of the Froude number and the sequent depth ratio:

$$\frac{h_2}{h_1} = 1.162 + 0.739(F_1) \tag{18}$$

$$\frac{L_j}{h_1} = 0.838 + 2.526\,(F_1) + 3.545\left(\frac{h_2}{h_1}\right) \tag{19}$$

$$\frac{L_r}{h_1} = -7.019 + 1.540\,(F_1) + 3.301\left(\frac{h_2}{h_1}\right) \tag{20}$$

To estimate the length of the hydraulic jump (L_j/h_1), Houichi et al. [19] introduced Eq. (1). A comparison of statistical indices results obtained by numerical simulation with Eq. (1) is shown in Table 6. In addition, the length of the hydraulic jump is predicted using Eqs. (19) and (1) as illustrated in Fig. 7. For the equation developed by Houichi et al, the correlation coefficient is calculated equal to 0.050 and also the MAPE, RMSE values are estimated 1242.576 and 244.050%, respectively. Equation (19) predicts the length of the hydraulic jump, (L_j/h_1), with more accuracy compared to the equation developed by Houichi et al. The MAPE, RMSE and R^2 values are computed by Eq. (19) 16.659, 3.606 and 0.946%, respectively.

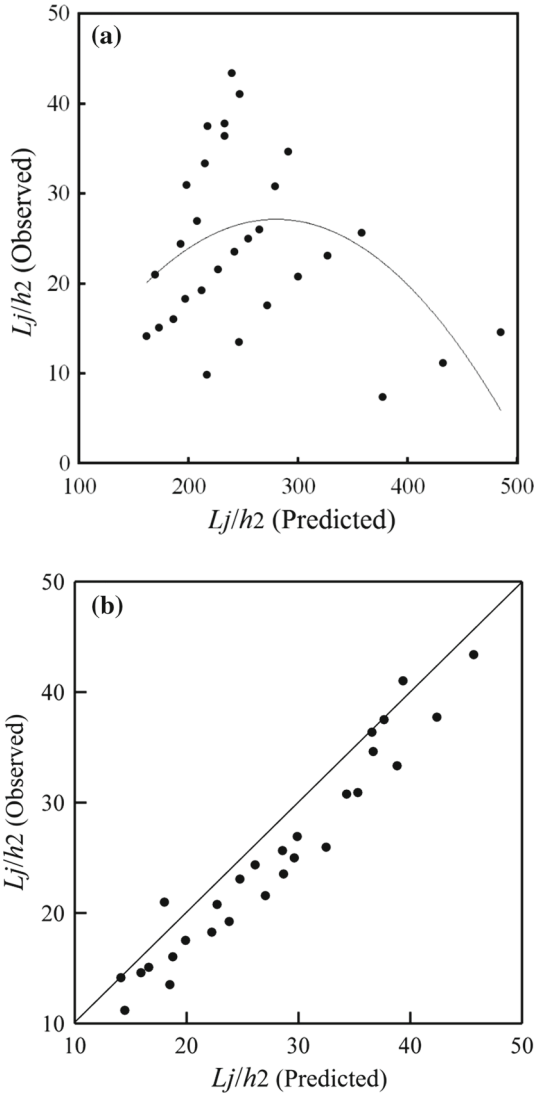

Fig. 7 Comparison of the length of hydraulic jump (L_j/h_1) for **a** Eq. (1), **b** Eq. (19)

8 Conclusion

Generally, after hydraulic structures such as ogee spillways, control gates and weirs the hydraulic jump occurs. A hydraulic jump is the rapid transition from a supercritical to subcritical flow. This transition is characterized by large-scale turbulence and energy dissipation. The most important parameters of a hydraulic jump are: the sequent depth, jump length and roller length ratios. In this study, the 3D pattern of hydraulic jumps in U-shaped channels was simulated using the FLOW-3D software. The 3D changes in the flow free surface were predicted using the volume of fluid (VOF) method. Also, the flow field turbulence was modeled using the standard $k-\varepsilon$ and RNG $k-\varepsilon$ turbulence models. According to the numerical model results, the standard $k-\varepsilon$ turbulence model predicted the changes in the flow free surface with more accuracy. For the hydraulic jump with $q = 0.166$, $F_1 = 5.3$, the standard $k-\varepsilon$ turbulence model calculated MAPE and RMSE 16.066 and 0.032, respectively. In contrast, the RNG $k-\varepsilon$ turbulence model predicted the MAPE and RMSE values about 1.33 and 1.53 times the standard $k-\varepsilon$ turbulence model, respectively. The comparison between the flow free surface variations of the simulated results with the experimental measurements showed a good accuracy of the numerical model. For example, for the hydraulic jump model with $q = 0.063$, $F_1 = 3.3$, the values of MAPE and RMSE and the correlation coefficient were calculated about 9.904, 0.008 and 0.925, respectively. Also, the numerical model estimated the values of RMSE and the correlation coefficient for the sequent depth ratio (h_2/h_1) 0.772 and 0.963, respectively. According to the modeling results, the average discrepancy

ratio value for the jump length ratio (L_j/h_1) was calculated 1.154. The changes in the sequent depth, the hydraulic jump length and the roller length ratios were studied for a range of Froude numbers from 1.93 to 8.85 and some relationships were provided to calculate these parameters. In this paper, the relationship of the sequent depth ratio is a function of the flow Froude number and the equations of the hydraulic jump and the roller length ratios are suggested in terms of the Froude number and the sequent depth ratio.

References

1. Rouse, H.; Siao, T.T.; Nagaratnam, S.: Turbulence characteristics of the hydraulic jumps. Trans. ASCE **124**(1), 926–950 (1959)
2. Rao, N.S.; Rajaratnam, N.: The submerged hydraulic jump. J. Hydraul. Div. **89**(1), 139–162 (1963)
3. McCorquodale, J.A.: Hydraulic jumps and internal flows. Encycl. Fluid. Mech **2**, 120–173 (1986)
4. Long, D.; Steffler, P.M.; Rajaratnam, N.: LDA study of flow structure in submerged hydraulic jump. J. Hydraul. Res. **28**(4), 437–460 (1990)
5. Svendsen, I.A.; Veeramony, J.; Bakunin, J.; Kirby, J.T.: The flow in weak turbulent hydraulic jump. J. Fluid Mech. **418**, 25–57 (2000)
6. Liu, M.; Rajaratnam, N.; Zhu, D.: Turbulence structure of hydraulic jumps of low froude numbers. J. Hydraul. Eng. **130**, 511–520 (2004)
7. Hager, W.H.: Hydraulic jump in non-prismatic rectangular channels. J. Hydraul. Res. **23**(1), 21–35 (1985)
8. Hager, W.H.; Wanoschek, R.: Hydraulic jump in triangular channel. J. Hydraul. Res. **25**(5), 549–564 (1987)
9. Debabeche, M.; Cherhabil, S.; Hafnaoui, A.; Achour, B.: Hydraulic jump in a sloped triangular channel. Can. J. Civ. Eng. **36**(4), 655–658 (2009)
10. Vatankhah, A.R.; Omid, M.H.: Direct solution to problems of hydraulic jump in horizontal triangular channels. Appl. Math. Lett. **23**, 1104–1108 (2010)
11. Rashwan, I.M.H.: Analytical solution to problems of hydraulic jump in horizontal triangular channels. Ain Shams Eng. J. **4**, 365–368 (2013)
12. Wanoschek, R.; Hager, W.H.: Hydraulic jump in trapezoidal channel. J. Hydraul. Res. **27**(3), 429–446 (1989)
13. Afzal, N.; Bushra, A.: Structure of the turbulent hydraulic jump in a trapezoidal channel. J. Hydraul. Res. **40**(2), 205–214 (2002)
14. Hager, W.H.: Hydraulic jump in U-shaped channel. J. Hydraul. Eng. **115**(5), 667–675 (1989)
15. Stahl, H.; Hager, W.H.: Hydraulic jump in circular pipes. Can. J. Civ. Eng. **26**, 368–373 (1999)
16. Bushra, A.; Afzal, N.: Hydraulic jump in circular and U-shaped channels. J. Hydraul. Res. **44**(4), 567–576 (2006)
17. Ghomri, A.; Debabeche, M.; Riguet, F.: Experimental study of hydraulic jump evolving in an u-shaped channel, with rough bed. J. Fundam. Appl. Sci. **1**(2), 82–105 (2009)
18. Zhang, Z.; Li, R.: Research on critical water depth, froude number and hydraulic jump of U-shaped channel. J. Xi'an Univ. Technol. **2**, 014 (2012)
19. Houichi, L.; Dechemi, N.; Heddam, S.; Achour, B.: An evaluation of ANN methods for estimating the lengths of hydraulic jumps in U-shaped channel. J. Hydroinform. **15**(1), 147–154 (2013)
20. Abdel-Gawad, S.M.; McCorquodale, J.A.: Analysis of the submerged radial hydraulic jump. Can. J. Civ. Eng. **12**(3), 593–602 (1985)
21. Sakarya, A.B.A.; Tokyay, N.D.: Numerical simulation of A-type hydraulic jumps at positive steps. Can. J. Civ. Eng. **27**(4), 805–813 (2000)
22. Zhao, Q.; Misra, S.K.; Svendsen, I.A.; Kirby, J.T.: Numerical study of a turbulent hydraulic jump. In: Proc. 17th Eng. Mech. Div. Conf. Vancouver (2004)
23. Federico, I.; Marrone, S.; Colagrossi, A.; Aristodemo, F.; Antuono, M.: Simulating 2D open-channel flows through an SPH model. Eur. J. Mech. B Fluids **34**, 35–46 (2012)
24. Rostami, F.; Shahrokhi, M.; MdSaod, M.; Sabbagh Yazdi, S.R.: Numerical simulation of undular hydraulic jump on smooth bed using volume of fluid method. J. Appl. Math. Model. **37**(3), 1514–1522 (2013)
25. Azimi, H.; Shabanlou, S.: The flow pattern in triangular channels along the side weir for subcritical flow regime. Flow Meas. Instrum. **46**, 170–178 (2015)
26. Azimi, H.; Hadad, H.; Shokati, Z.; Salimi, M.S.: Discharge and flow field of the circular channel along the side weir. Can. J. Civ. Eng. **42**(4), 273–280 (2015)
27. Azimi, H.; Shabanlou, S.: Comparison of subcritical and supercritical flow patterns within triangular channels along the side weir. Int. J. Nonlinear Sci. Numer. **17**(7–8), 361–368 (2016)
28. Azimi, H.; Shabanlou, S.; Ebtehaj, I.; Bonakdari, H.: Discharge coefficient of rectangular side weirs on circular channels. Int. J. Nonlinear Sci. Numer. **17**(7–8), 391–399 (2016)
29. Mahmodinia, S.; Javan, M.; Eghbalzadeh, A.: The flow field and free surface pattern of the submerged side weir with different lengths. Arab. J. Sci. Eng. **39**(6), 4461–4472 (2014)
30. Shekari, Y.; Javan, M.; Eghbalzadeh, A.: Three-dimensional numerical study of submerged hydraulic jumps. Arab. J. Sci. Eng. **39**(10), 6969–6981 (2014)
31. FLOW 3D User's Manual.; (2011). Version 10.0. Flow Science Inc
32. Hirt, C.W.; Nichols, B.D.: Volume of fluid (VOF) method for the dynamics of free boundaries. J. Comput. Phys. **39**(5), 201–225 (1981)